

# Mathematical Model of Forced Vibration in Pre-stressed Piezoelectric Plate-Strips Resting on Rigid Foundation

**Ahmet Daşdemir**

Department of Mathematics, Faculty of Arts and Sciences, Kastamonu University  
Kuzeykent Campus, 37150 Kastamonu, Turkey  
e-mail: ahmetdasdemir37@gmail.com

Article history

Received: 21 September 2017

Received in revised form: 29 March 2018

Accepted: 2 April 2018

Published on line: 1 December 2018

---

**Abstract** A mathematical model is presented to investigate the dynamics of a pre-stressed piezoelectric plate-strip resting on a rigid foundation, under the action of a time-harmonic force, utilizing the three-dimensional linearized theory of electro-elastic waves in initially stressed bodies. The governing equations of motion are solved by employing the finite element method, and numerical results illustrating the relations between different problem parameters are investigated. In particular, we show that the initial tension of the plate-strip prevents its resonance, but the compression force passes after the corresponding resonance mode.

**Keywords** Piezoelectric material; finite element method; time-harmonic force; plate-strip; forced vibration; rigid foundation

**Mathematics Subject Classification** 74H45, 74S05

## 1 Introduction

The mechanical investigation of piezoelectric materials is becoming increasingly important, as they are being used in more and more sophisticated areas such as beams, plates, and shells. In the past few years, there has been tremendous interest in studying the mechanical behavior of such materials. A review of the most well-known investigations is given in [1].

Many studies have been devoted to investigating such mechanical problems. Nowacki *et al.* [2] investigated a structure comprising a piezoelectric layer on a piezoelectric substrate. Considering the usual negative-velocity feedback control law, Wang *et al.* [3] investigated the dynamic stability of active vibration control for piezoelectric composite plates. Kochetkov and Rogacheva [4] presented approximate solutions for three-dimensional problems involving piezoelectric actuators and sensors attached to elastic bodies Qing *et al.* [5] created a new and effective analysis method for dynamic problems involving piezoelectric plates. Liou and Sung [6] studied a problem arising at an anisotropic piezoelectric half-plane boundary under electrical (mechanical) loading. Hosseini-Hashemi *et al.* [7] considered the three-dimensional natural

frequencies of circular and annular functionally-graded plates with the addition of two piezoelectric layers. Akbarov and Ilhan [8] investigated Lamb's problem for a structure comprising a piezoelectric layer on a piezoelectric half-plane under a time-harmonic force located at a point. Li *et al.* [9] modeled a problem involving a laminated composite plate with piezoelectric layers bonded to its upper and lower surfaces using third-order shear deformation plate theory.

Due to the advantages offered by piezoelectric materials, various problems have been investigated using suitable numerical methods. However, these problems depend significantly on certain factors that make it difficult to solve them because they give rise to non-linear effects in the dynamics of the elastic medium. These factors include (a) the choice of materials and (b) the initial static stresses in each layer that are present before the external dynamical force is applied. The first factor (a) is one of the most significant ones affecting the systems dynamics. The initial stresses in the body's layers (factor b) may arise either due to technological requirements or due to the temperature of the environment. Note that the classical linear theory of elastodynamics is often inadequate for solving such problems, due to these and similar factors. Since the wave propagation exhibits non-linear effects, deformations in elastic bodies are consequently governed by a set of nonlinear partial differential equations. Assuming that (i) the pre-stressed state (or initial stress) is exactly homogeneous and static and (ii) the additional dynamic load to which the pre-stressed body is subjected is significantly smaller than the magnitude of the initial load, these issues can be handled by the three-dimensional linearized theory of elastic waves in initially stressed bodies. For further details, see references [10] and [11].

This paper presents a mathematical model of the dynamic stress field problem for a pre-stressed piezoelectric plate-strip resting on a rigid foundation under the influence of a time-harmonic force, assuming a piecewise-homogeneous body model and utilizing of the three-dimensional linearized theory of electro-elastic waves in initially stressed bodies (TLTEEWISB). This model is solved by employing the finite element method (FEM). In particular, certain problem parameters relevant to the frequency response of the plate-strip are discussed and analyzed.

## 2 Mathematical Model

Consider a pre-stressed piezoelectric plate-strip, poled along the  $Ox_2$ -axis direction with thickness  $h$  and length  $2a$ , resting on a rigid foundation, as shown in Figure 1. We associate it with Lagrange coordinates denoted by  $x_i'$  which, in the natural state, coincide with Cartesian coordinates  $x_i$ . It is assumed that the plate-strip is in complete contact with the rigid foundation. A time-harmonic force is applied to the midpoint of the plate-strip's free surface, and this point is chosen as the origin of the coordinate axes. It should be noted that the length of the plate-strip in the  $Ox_3$ -axis direction is infinite, and it is assumed that the applied time-harmonic force extends to infinity in that direction. As a result, plane deformation arises in the  $Ox_1x_2$ -plane. Hence, all numerical investigations will involve the region

$$B = \{(x_1, x_2) : -a \leq x_1 \leq a, -h \leq x_2 \leq 0\}. \quad (1)$$

Before the plate-strip is attached to the rigid foundation, it is stretched or compressed separately in the  $Ox_1$ -axis directions by a uniformly distributed normal force, producing a uniaxial homogenous initial stress state in the plate-strip. This initial stress can be determined

using the linear theory of electro-elasticity as follows:

$$\sigma_{11}^0 = q \text{ and } \sigma_{12}^0 = \sigma_{13}^0 = 0, \tag{2}$$

where  $q$  is a known constant, and the additional superscript “0” represents the corresponding initial stress intensity. The character of piezoelectric materials mean that the following initial axial homogeneous electric displacement emerges in the piezoelectric layer:

$$D_1^0 = d \text{ and } D_2^0 = 0, \tag{3}$$

where  $d$  is a known constant. Note that the initial stress and electric displacement cannot be independent of each other, as they must be self-consistent. This will be discussed in more detail later.

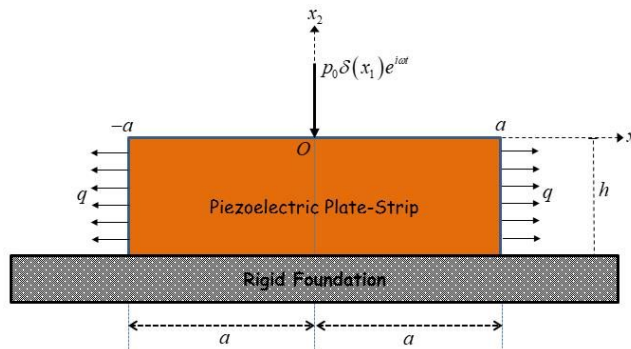


Figure 1: Schematic of Plate-strip Problem

According to Yang [1] and Guz [10, 11], the electro-elastic response of a piezoelectric plate-strip is governed by the dynamic and electrostatic equilibrium equations

$$\sigma_{ij,j} + qu_{i,11} = \rho \ddot{u}_i \tag{4}$$

and

$$D_{i,i} + du_{i,i1} = 0, \tag{5}$$

where  $i, j = 1, 2$ ,  $\sigma_{ij}$  is the symmetric stress tensor,  $D_i$  is electric displacement vector,  $u_i$  is the mechanical displacement with respect to  $x_i$ , and  $\rho$  is the mass density in its natural state. The dots over the displacement components represent differentiation with respect to time, and a comma followed by a subscript represents differentiation with respect to the relevant space-coordinate. Here and below, repeated subscript indices are summed with respect to all possible index values. The mechanical and geometrical relations for the present case can be written as follows.

$$\begin{aligned} \sigma_{11} &= c_{11}u_{1,1} + c_{13}u_{2,2} + e_{31}\varphi_{,2} \\ \sigma_{22} &= c_{13}u_{1,1} + c_{33}u_{2,2} + e_{33}\varphi_{,2} \\ \sigma_{12} &= \sigma_{21} = c_{44}(u_{1,2} + u_{2,1}) + e_{15}\varphi_{,1} \\ D_1 &= e_{15}(u_{1,2} + u_{2,1}) - \gamma_{11}\varphi_{,1} \\ D_2 &= e_{31}u_{1,1} + e_{33}u_{2,2} - \gamma_{33}\varphi_{,2} \end{aligned} \tag{6}$$

Here, the  $c_{ij}$ 's are elastic constants, the  $e_{ij}$ 's are piezoelectric constants,  $\varphi$  is the electric field potential, and the  $\gamma_{ik}$ 's are dielectric constants.

Now the boundary and contact conditions are considered. According to the foregoing discussion, the boundary-contact conditions can be given as

$$\sigma_{21}|_{x_2=0} = 0, \quad \sigma_{22}|_{x_2=0} = -p_o \delta(x_1) e^{i\omega t}, \quad (7)$$

$$(qu_{j,1} + \sigma_{1j})|_{x_1=\mp a} = 0, \quad (8)$$

$$u_j|_{x_2=-h} = 0 \quad (9)$$

and

$$(D_i + u_{i,j} D_j^0)|_{x_1=\mp a} = 0, \quad (10)$$

where  $\delta(\cdot)$  is the Dirac delta function. In addition, the electrically open conditions can be written in the form

$$\varphi|_{x_1=\mp a} = 0 \text{ and } \varphi|_{x_2=0,-h} = 0. \quad (11)$$

This completes the formulation of the problem and the investigation of the governing field equations.

### 3 Solution Procedure

As the structure of this problem is quite complex, it cannot be solved analytically. Consequently, the FEM is employed here to provide a solution. First, however, some preparation is necessary. The dimensionless coordinate system is introduced:

$$\hat{x}_1 = \frac{x_1}{h} \text{ and } \hat{x}_2 = \frac{x_2}{h}. \quad (12)$$

Since the force is assumed to be time-harmonic, with frequency  $\omega$ , and can be represented as  $p_o \delta(x_1) e^{i\omega t}$ , all the corresponding dependent variables can be represented as

$$\{\sigma_{ij}, u_i, \varepsilon_{ij}, D_i\}(x_1, x_2, t) = \{\bar{\sigma}_{ij}, \bar{u}_i, \bar{\varepsilon}_{ij}, \bar{D}_i\}(x_1, x_2) e^{i\omega t}, \quad (13)$$

where the over bars denote the amplitudes of the corresponding quantities. After applying the coordinate transformation (12) and substituting the expression (13) into the foregoing equations and conditions, the equivalent equations and boundary-contact conditions can be obtained for the amplitudes of the sought values by replacing the terms  $\partial^2 u_j / \partial t^2$  and  $p_o \delta(x_1) e^{i\omega t}$  with  $-\omega^2 u_j$  and  $p_o \delta(x_1)$ , respectively. Hereafter, we will omit the superimposed dashes and hats until specified otherwise.

Now, to present the FEM model for this boundary-contact problem, the functional

$$J(\mathbf{u}, \varphi) = J(\mathbf{u}) + J(\varphi) \quad (14)$$

is proposed, where

$$J(\mathbf{u}) = \frac{1}{2} \int_B \left[ \tilde{c}_1 \left( \frac{\partial u_1}{\partial x_1} \right)^2 + \tilde{c}_3 \left( \frac{\partial u_2}{\partial x_2} \right)^2 + \left( \frac{\partial u_1}{\partial x_2} + \frac{\partial u_2}{\partial x_1} \right)^2 + 2\tilde{c}_2 \frac{\partial u_1}{\partial x_1} \frac{\partial u_2}{\partial x_2} \right] dB \quad (15)$$

$$+ \int_S \frac{p_o}{c_{44}} \delta(x_1) u_2 dS_2$$

and

$$J(\varphi) = \frac{1}{2} \int_B \left[ 2\tilde{e}_5 \left( \frac{\partial u_1}{\partial x_2} + \frac{\partial u_2}{\partial x_1} \right) \frac{\partial \varphi}{\partial x_1} + 2 \left( \tilde{e}_1 \frac{\partial u_1}{\partial x_1} + \tilde{e}_3 \frac{\partial u_2}{\partial x_2} \right) \frac{\partial \varphi}{\partial x_2} \right. \\ \left. + \kappa \left( \frac{\partial u_2}{\partial x_1} \frac{\partial \varphi}{\partial x_2} + \frac{\partial u_1}{\partial x_1} \frac{\partial \varphi}{\partial x_1} \right) - \tilde{\gamma}_1 \left( \frac{\partial \varphi}{\partial x_1} \right)^2 - \tilde{\gamma}_3 \left( \frac{\partial \varphi}{\partial x_2} \right)^2 \right] dB. \quad (16)$$

In Equation (15),  $S$  represents the boundary enclosing domain  $B$ , and Equation (15) and Equation (16) introduce the following notation:

$$\tilde{c}_1 = \frac{c_{11}}{c_{44}}, \quad \tilde{c}_2 = \frac{c_{13}}{c_{44}}, \quad \tilde{c}_3 = \frac{c_{33}}{c_{44}}, \quad \eta = \frac{q}{c_{44}}, \quad \Omega = \omega h \sqrt{\frac{\rho}{c_{44}}}, \\ \tilde{e}_1 = \frac{e_{31}}{c_{44}}, \quad \tilde{e}_3 = \frac{e_{33}}{c_{44}}, \quad \tilde{e}_5 = \frac{e_{15}}{c_{44}}, \quad \tilde{\gamma}_1 = \frac{\gamma_{11}}{c_{44}}, \quad \tilde{\gamma}_3 = \frac{\gamma_{33}}{c_{44}}, \quad \kappa = \frac{d}{2c_{44}}. \quad (17)$$

Here,  $\Omega$  is the dimensionless frequency of the plate-strip and  $\eta$  is the initial stress parameter.

The validity of the proposed functional (14) can be proven using the fundamental principles of the calculus of variations as follows. Its first variation, denoted by  $\delta J(\mathbf{u}, \varphi) = 0$ , must be computed, and then the coefficients of the terms  $\delta u_1$ ,  $\delta u_2$ , and  $\delta \varphi$  must separately be set equal to zero. Using this procedure, the equations of motion (4)-(5) and the boundary-contact conditions (7)-(11) can be derived, completing the proof.

The FEM model can now be created, according to the virtual work principle and the standard Rayleigh-Ritz method [12]. To do this, the domain  $B$  is divided into a number of subdomains with smooth rectangular structures. The number of these finite elements is such that the boundary conditions are satisfied with very high accuracy and the numerical results converge sufficiently well. Let the mechanical displacements and the electric field potential for the  $t$ th finite element be

$$u_1^{(t)} = \sum_{i=1}^M \alpha_i^{(t)} N_i(r, s) \quad u_2^{(t)} = \sum_{i=1}^M \beta_i^{(t)} N_i(r, s) \quad \text{and} \quad \varphi^{(t)} = \sum_{i=1}^M \phi_i^{(t)} N_i(r, s), \quad (18)$$

where  $M$  is number of the nodes in the  $t$ th finite element, the coefficients  $\alpha_i^{(t)}$ ,  $\beta_i^{(t)}$  and  $\phi_i^{(t)}$  are unknowns that need to be determined, the  $N_i(r, s)$  are the shape functions for the  $t$ th finite element, and  $r$  and  $s$  are the local normalized coordinate components in the local coordinate system associated with the corresponding element. Note that the shape functions are chosen such that  $N_j(r, s) \in L_2^1$ , where  $L_2^1$  is the set of functions whose squares and first order partial differentials are Lebesgue integrable. The shape functions are defined over the domain  $[-1, 1] \times [-1, 1]$ .

Substituting Equation (18) into Equation (14) and applying the usual solution method to the resultant equation leads to the following system of algebraic equations, in matrix form:

$$(\mathbf{K} - \omega^2 \mathbf{M}) \tilde{\mathbf{x}} = \mathbf{F} \quad (19)$$

where  $\mathbf{K}$  is the stiffness matrix,  $\mathbf{M}$  is the mass matrix,  $\tilde{\mathbf{x}}$  is a column vector representing the unknown displacements and the electric field potential, and  $\mathbf{F}$  is the force vector. To reduce the size of the present paper, the explicit forms of the matrices and vectors in (19) are not given here, but they can be derived directly from Equation (14)-(17) using this procedure.

The displacements and electric field potentials at the nodes can now be obtained by solving the matrix equation (19). Given these values, the stresses can easily be calculated using the stress-displacement relation

$$\tilde{\sigma} = \mathcal{D}\mathcal{B}\tilde{\mathbf{x}} \quad (20)$$

where

$$\tilde{\sigma} = \left[ \begin{array}{ccccc} \sigma_{11} & \sigma_{22} & \sigma_{12} & D_1 & D_2 \end{array} \right]^T \quad (21)$$

$$\mathcal{D} = \left[ \begin{array}{ccccc} c_{11} & c_{13} & 0 & 0 & e_{31} \\ c_{13} & c_{33} & 0 & 0 & e_{33} \\ 0 & 0 & c_{44} & e_{15} & 0 \\ 0 & 0 & e_{15} & -\gamma_{11} & 0 \\ e_{31} & e_{33} & 0 & 0 & -\gamma_{33} \end{array} \right] \quad (22)$$

and

$$\mathcal{B} = \left[ \begin{array}{ccccccccc} \frac{\partial N_1}{\partial r} & \dots & \frac{\partial N_M}{\partial r} & 0 & \dots & 0 & 0 & \dots & 0 \\ 0 & \dots & 0 & \frac{\partial N_1}{\partial s} & \dots & \frac{\partial N_M}{\partial s} & 0 & \dots & 0 \\ \frac{\partial N_1}{\partial s} & \dots & \frac{\partial N_M}{\partial s} & \frac{\partial^2 N_1}{\partial r \partial s} & \dots & \frac{\partial^2 N_M}{\partial r \partial s} & 0 & \dots & 0 \\ 0 & \dots & 0 & 0 & \dots & 0 & \frac{\partial N_1}{\partial r} & \dots & \frac{\partial N_M}{\partial r} \\ 0 & \dots & 0 & 0 & \dots & 0 & \frac{\partial N_1}{\partial s} & \dots & \frac{\partial N_M}{\partial s} \end{array} \right]. \quad (23)$$

This completes the discussion of the FEM model of the considered problem.

## 4 Numerical Results and Discussion

Before presenting the numerical results, some explanation are necessary. Here, the body being considered was divided into 200 equal parts along the  $Ox_1$ -axis direction, denoted by  $m$ , and into 20 equal parts in the  $Ox_2$ -axis direction, denoted by  $n$ , unless stated otherwise. The mechanical, piezoelectric, and dielectric constants of the materials used for the body are given in Table 1 [13]. All the numerical investigations were made at the interface between the plate-strip and the rigid foundation, with  $h/2a = 0.2$ ,  $\Omega = 0$ , and  $\eta = 0$ . The ratios  $C_{pq} = \tilde{c}_p/\tilde{c}_q$  and  $\Gamma = \tilde{\gamma}_1/\tilde{\gamma}_3$  have also been introduced. Unless stated otherwise, BaTiO<sub>3</sub> will be used for the concrete examples. As previously discussed, a self-consistency condition on the initial stress (tension or compression) field for the piezoelectric phase must be satisfied. In this study, only a uniformly distributed normal initial stress field is considered. By considering the constitutive equations given in (6), this means that the equation  $d = q(c_{13}e_{33} - c_{33}e_{31}) / (c_{13}^2 - c_{11}c_{33})$  can be directly obtained for the piezoelectric phase.

The validity and reliability of the algorithms and PC programs used for the considered problem must also be verified. To do this, an error analysis was made by employing the function

$$\Delta_{case}\bar{f} = |f(\text{constant}) - f(\text{variable})|,$$

and it was shown that the boundary-contact conditions (7)-(11) were satisfied and that the numerical results obtained agreed well with the foregoing mathematical, mechanical and physical considerations.

Figure 2 shows how the function  $\Delta_m\bar{\sigma}_{22} = |\sigma_{22}|_{m=200} - \sigma_{22}|_{m<200}| \times h/p_0$  varies with respect to  $x_1/h$ . It can be concluded from this figure that, by increasing the number of finite elements in the  $Ox_1$ -axis direction, the error function values tend to zero. Figure 3 show the variation

Table 1: Mechanical, Piezoelectric, and Dielectric Constants for Various Materials

Materials	$c_{11}$	$c_{13}$	$c_{33}$	$c_{44}$	$e_{31}$	$e_{33}$	$e_{15}$	$\gamma_{11}$	$\gamma_{33}$
	$\times 10^{10}$ (N/m <sup>2</sup> )				(C/m <sup>2</sup> )			$\times 10^{-8}$ (F/m)	
BaTiO <sub>3</sub>	15.0	6.6	14.6	4.4	-4.35	17.5	11.4	1.115	1.26
NBS-1	11.0	4.12	10.0	3.45	-3.3	14.8	7.7	0.9	0.89
PCR-8	14.4	7.7	11.6	2.83	-7.5	13.6	11.6	0.83	0.74
TBKS	14.6	5.06	14.2	4.9	-0.68	7.71	4.56	0.41	0.336
TBK-3	15.7	6.2	15.3	4.4	-3.2	12.5	9.1	0.95	0.95

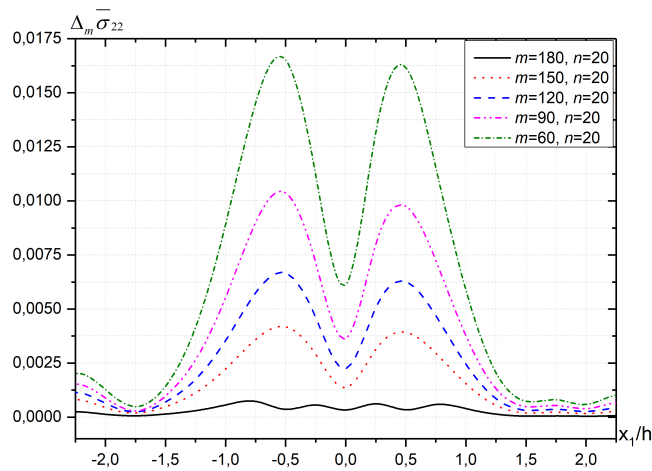


Figure 2: Distribution of the Function  $\Delta_m \bar{\sigma}_{22}$  for  $h/2a = 0.2$ ,  $\Omega = 0$ , and  $\eta = 0$

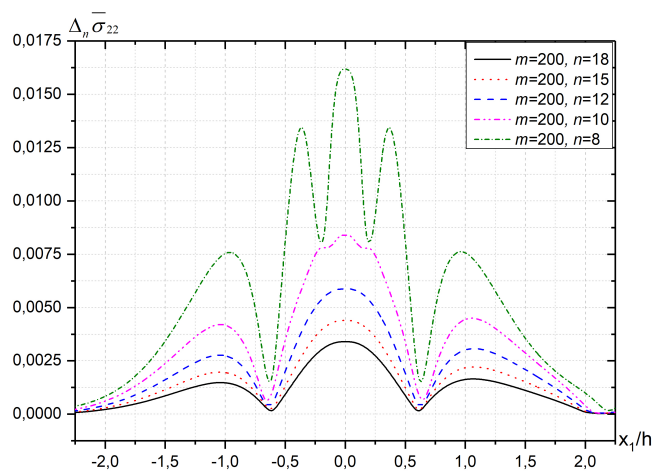


Figure 3: Distribution of the Function  $\Delta_n \bar{\sigma}_{22}$  for  $h/2a = 0.2$ ,  $\Omega = 0$ , and  $\eta = 0$

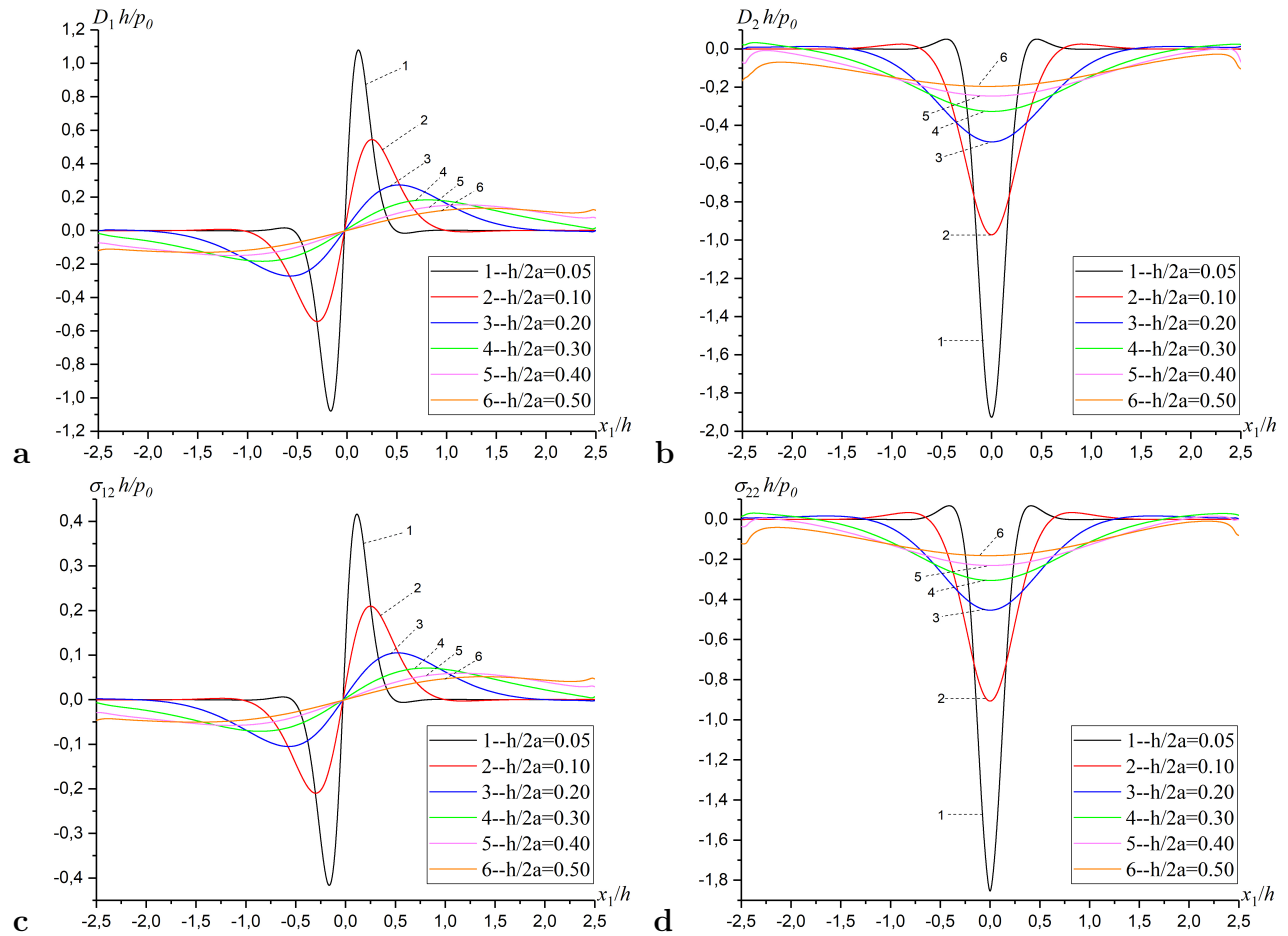


Figure 4: Effect of the Thickness ratio on the Distribution of **a**  $D_1 h/p_0$ , **b**  $D_2 h/p_0$ , **c**  $\sigma_{12} h/p_0$ , **d**  $\sigma_{22} h/p_0$  for PCR - 8, for  $\Omega = 0.1$  and  $\eta = 0$

in the function  $\Delta_n \bar{\sigma}_{22} = |\sigma_{22}|_{n=20} - \sigma_{22}|_{n<20}| \times h/p_0$ , demonstrating that the value of the function  $\Delta_n \bar{\sigma}_{22}$  decreases as the number of finite elements in the  $Ox_2$ -axis direction increases. Consequently, increasing the number of finite elements leads to an improvement in the numerical results obtained by the current algorithm. Moreover, comparing the graphs given in Figs. 2 and 3 reveals the following.

- By increasing the value of  $m$ , the absolute error at the point  $x_1/h = 0$ , i.e., the point where the force is applied to the plate-strip, quickly tends to zero, and the absolute maximum error values are obtained near the points  $x_1/h = \mp 0,5$ .
- In contrast to increasing the value of  $m$ , increasing the value of  $n$  causes the absolute errors to reach a maximum at the point  $x_1/h = 0$ , and to vanish around the points  $x_1/h = \mp 0,5$ .

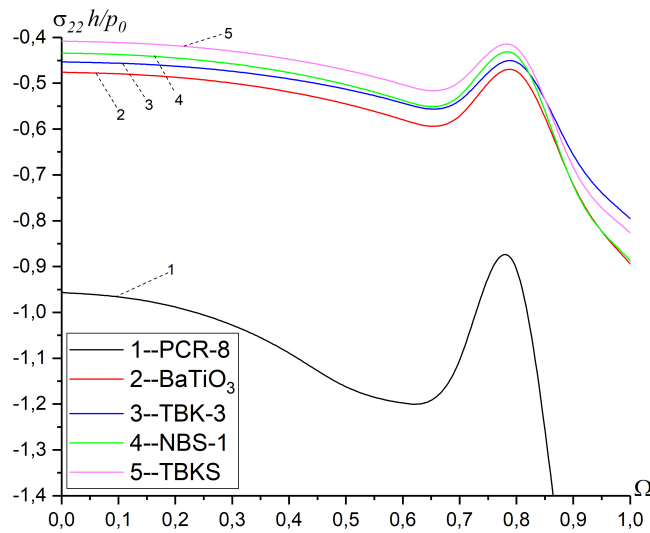


Figure 5: Relationship between  $\sigma_{22}h/p_0$  and  $\Omega$  for Various Materials, for  $h/2a = 0.2$  and  $\eta = 0$

Figure 4 shows the distributions of the electric displacements  $D_1h/p_0$  (Figure 4a) and  $D_2h/p_0$  (Figure 4b), the shear stress  $\sigma_{12}h/p_0$  (Figure 4c) and the normal stress  $\sigma_{22}h/p_0$  (Figure 4d) with respect to  $x_1/h$  for different piezoelectric material thickness ratios. From this, it can be seen that the stress distributions and electric displacements gradually decrease as the thickness ratios increases. Increasing the ratio  $h/2a$  leads to decreasing oscillation in the stress and electric displacements components. It should be noted that the changes in the shear stress  $\sigma_{12}h/p_0$  with the electric displacement  $D_1h/p_0$  and in the normal stress  $\sigma_{22}h/p_0$  with the electric displacement  $D_2h/p_0$  have the same vibrational characteristics. Formally, the graphs of both the shear stress and the electric displacement  $D_1h/p_0$  in the  $Ox_1$ -axis direction are symmetric with respect to the origin, while the others are symmetric with respect to  $x_1/h = 0$ .

The numerical results obtained in Figure 2 and Figure 3 are expected, due to the solution procedure used. Furthermore, the results in Figure 4 agree well with the foregoing mechanical considerations. In addition, the distributions of the stresses and electric displacements vanish toward to the edges of the graphs. Note that these figures are for media with no initial stress. Hence, the numerical results satisfy the boundary conditions (8), proving the validity and reliability of the algorithms and PC programs.

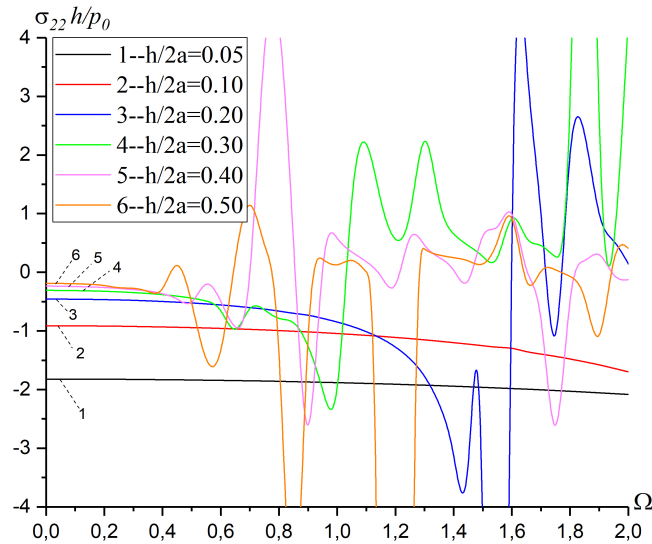


Figure 6: Relationship between  $\sigma_{22}h/p_0$  and  $\Omega$  for various values of  $h/2a$ , for  $\eta = 0$

The main aim of this paper is to investigate the effect of certain parameters on the plate-strip frequency response of the plate-strip strip, so all graphs will be plotted for the point  $(0, -1)$  from now on.

Figure 5 shows the effect of the choice of plate-strip material on the relationship between  $\sigma_{22}h/p_0$  and  $\Omega$ , indicating that this relationship is non-monotonic. This result agrees well with the foregoing mechanical considerations. For each material, the absolute value of the normal stress  $\sigma_{22}h/p_0$  increases with the parameter  $\Omega$  up to a certain value, specific to that material. It can also be observed that the absolute value of  $\sigma_{22}h/p_0$  reaches a maximum for certain values of  $\Omega$ . These values are called resonance values and are denoted by  $\Omega_{res}$ . These  $\Omega_{res}$  values decrease as the ratios  $C_{23}$  and  $\Gamma$  increase, but increase with the ratio  $C_{12}$ .

Figure 6 show how the stress  $\sigma_{22}h/p_0$  varies with respect to the dimensionless frequency  $\Omega$  for various thickness ratios  $h/2a$ . The  $\Omega_{res}$  values decrease as the ratio  $h/2a$  increases. Note that the  $\Omega_{res}$  values can be determined from the graphs. Increasing the thickness  $h/2a$  causes the number of local extrema of  $\sigma_{22}h/p_0$  to increase with respect to  $\Omega$ . The ratio  $h/2a$  has a significant effect on the plate-strips frequency response, not only quantitatively, but also qualitatively.

Figure 7 shows the relationship between the stress  $\sigma_{22}h/p_0$  and the dimensionless frequency  $\Omega$  when plate-strip experiences an initial compression or tension field. Note that the negative (positive) sign of the parameter  $\eta$  denotes initial compression (tension). These graphs indicates that increasing the value of the initial compression (tension) parameter  $\eta$  causes the absolute values of  $\sigma_{22}h/p_0$  to increase (decrease). The initial stretching prevents the resonance value of  $\sigma_{22}h/p_0$ , but the initial compressing exceeds the corresponding resonance value. As a result, the initial stress parameter  $\eta$  has a considerable influence on the frequency response of the stress  $\sigma_{22}h/p_0$ , not only quantitatively, but also in the qualitatively. Moreover, the numerical results show that there are locations where parametric resonance arises in the stress  $\sigma_{22}h/p_0$  for certain values of  $\eta$  as can be observed from the bottom box in the figure. An increase in the parameter  $\eta$  reduces these parametric resonances.

Figure 8 shows the effect of the material choice on the relationship between the stress

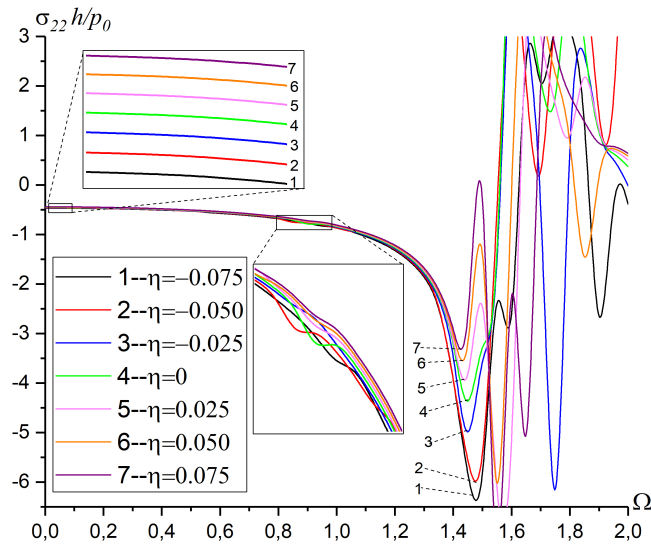


Figure 7: Relationship between  $\sigma_{22}h/p_0$  and  $\Omega$  for Various Values of  $\eta$ , for  $h/2a = 0.2$

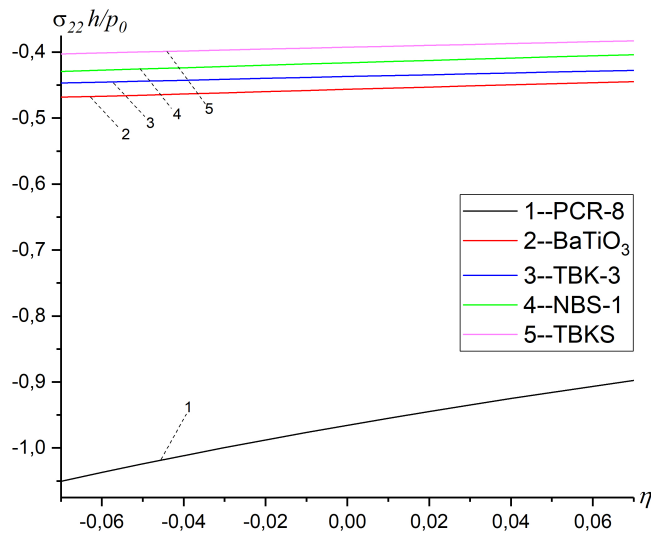


Figure 8: Relationship between  $\sigma_{22}h/p_0$  and  $\Omega$  for Various Materials, for  $h/2a = 0.2$  and  $\Omega = 0$

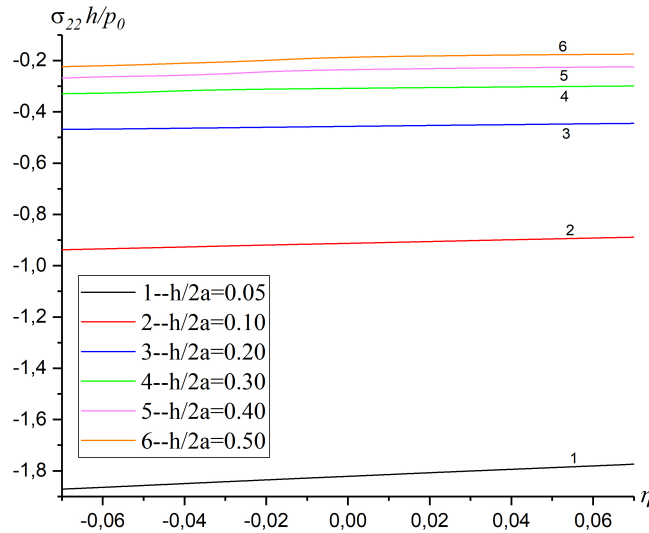


Figure 9: Relationship between  $\sigma_{22}h/p_0$  and  $\Omega$  for Various Values of  $h/2a$ , for  $\Omega = 0$

$\sigma_{22}h/p_0$  and the initial stress parameter  $\eta$ . In addition, Figure 9 shows the influence of  $h/2a$  on this relationship. Together, these figures demonstrate that the distribution of the stress  $\sigma_{22}h/p_0$  depends linearly on both the initial tension and compression. Increasing the  $h/2a$  value reduces the influence of on the distribution of  $\sigma_{22}h/p_0$ . Moreover, this influence decreases as the ratios  $C_{23}$  and  $\Gamma$  decrease, but as the ratio  $C_{12}$  increases.

## 5 Conclusion

This paper presents a mathematical model for investigating the forced vibration of a pre-stressed piezoelectric plate-strip resting on rigid foundation, subject to the action of a time-harmonic force, assuming a piecewise-homogeneous body model and utilizing the TLTEEWISB. This model was solved numerically by employing the FEM. Numerical results illustrating the influence of certain parameters on the dynamics of the considered plate-strip have been discussed, leading to the following important conclusions.

- Initial tension prevents resonance in the stress  $\sigma_{22}h/p_0$ , but initial compression passes after this resonance mode.
- For certain values of the initial stress parameter  $\eta$ , there are locations where parametric resonance occurs in the stress  $\sigma_{22}h/p_0$ .
- Decreasing the plate-strip's thickness for a given length causes the number of local extrema of the stress  $\sigma_{22}h/p_0$  to decrease;
- Increasing the  $h/2a$  value causes the influence of the initial stress  $\eta$  on the dispersion behavior of the stress  $\sigma_{22}h/p_0$  to decrease.

Although the numerical results given here have been presented for certain specific materials (e.g., PCR-8), they are more general valid in a qualitative sense. Moreover, these results are encountered in everyday engineering practice, in the impact treatment of metals resting on other metals.

## Acknowledgments

The author would like to thank the referees for constructive comments, which improved the presentation of the paper. This study was supported by the grant from Research Fund of Kastamonu University under project number KÜ-BAP01/2016-4.

## References

- [1] Yang, J. *An Introduction to the Theory of Piezoelectricity*. New York: Springer-Verlag. 2005.
- [2] Nowacki, J. P., Alshits, V. I. and Radowicz, A. 2D electro-elastic fields in a piezoelectric layer-substrate structure. *Internat. J. Engrg. Sci.* 2002. 40: 2057–2076.
- [3] Wang, S. Y., Quek, S. T. and Ang, K. K. Dynamic stability analysis of finite element modeling of piezoelectric composite plates. *Internat. J. Solids Structures. Internat. J. Engrg. Sci.* 2004. 41: 745–764.
- [4] Kochetkov, I. D. and Rogacheva, N. N. Contact interaction of a piezoelectric actuator and elastic half-space. *J. Appl. Math. Mech.* 2005. 69: 792–804.
- [5] Qing, G., Xu, J., Li, P. and Qiu, J. A new efficient numerical method and the dynamic analysis of composite laminates with piezoelectric layers. *Compos Struct.* 2007. 78: 457–467.
- [6] Liou, J. Y. and Sung, J. C. Electrostatic stress analysis of an anisotropic piezoelectric half-plane under surface electromechanical loading. *Internat. J. Solids Structures.* 2008. 39: 2547–2556.
- [7] Hosseini-Hashemi, Sh. Azimzadeh-Monfared, M. and Taher, H. R. D. A 3-D Ritz solution for free vibration of circular/annular functionally graded plates integrated with piezoelectric layers. *Internat. J. Engrg. Sci.* 2010. 48: 1971–1984.
- [8] Akbarov, S. D. and Ilhan, N. Time-harmonic Lamb’s problem for a system comprising a piezoelectric layer and piezoelectric half-plane. *J. Sound Vibration.* 2013. 332: 5375–5392.
- [9] Li, S., Huang, L., Jiang, L and Qin, R. A bidirectional B-spline finite point method for the analysis of piezoelectric laminated composite plates and its application in material parameter identification. *Compos Struct.* 2014. 107: 346–362.
- [10] Guz, A. N. *Elastic Waves in a Body Initial Stresses, I. General Theory*. Kiev: Naukova Dumka. 1986 (in Russian).
- [11] Guz, A. N. *Elastic Waves in a Body Initial Stresses, II. Propagation Laws*. Kiev: Naukova Dumka. 1986 (in Russian).
- [12] Zienkiewicz, O. C. and Taylor, R. L. *The Finite Element Method, Basic Formulation and Linear Problems*. London: McGraw-Hill. 1989.
- [13] Topolov, V. Y. and Bowen, C. R. *Electromechanical Properties in Composites Based on Ferroelectrics*. London: Springer. 2009.